Journal of Green Energy Research and Innovation

Introducing New Control Methods to Apply in Flexible Photovoltaic Systems at the 3-Phase 4-Wire Grids

Saeid Khani, Leila Mohammadian

Highlights

- **Presents a corrected p-q control strategy for PV systems in unbalanced, distorted 3-phase 4-wire grids.**
- **Combines PV with active power filtering to function as a flexible photovoltaic (FPV) system.**
- **Proposes enhanced vectorial control to mitigate harmonics, voltage unbalance, and reactive power.**
- **Ensures dynamic adaptability to disturbances while maintaining optimal MPPT power extraction.**
- **Integrates flexible distributed generation (FDG) models for multi-purpose grid stabilization.**

Graphical Abstract

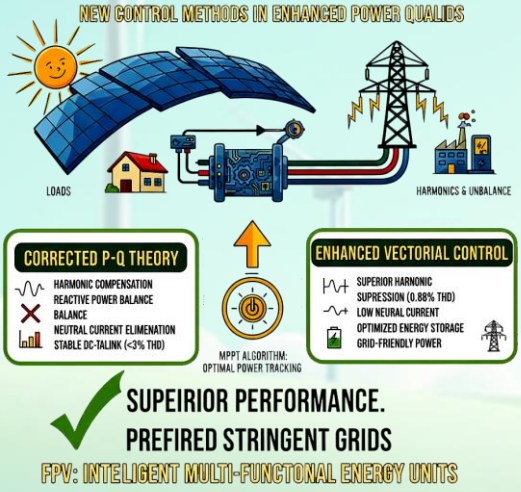

Use your device to scan and read the article online

Citation

S. Khani, and L. Mohammadian, "Introducing New Control Methods to Apply in Flexible Photovoltaic Systems at the 3-Phase 4-Wire Grids," *Journal of Green Energy Research and Innovation*, vol. 2, no. 4, pp. 27-44, 2025.

https://doi.org/10.61882/jgeri.2.4.27

Journal of Green Energy Research and Innovation 2.4 (2025) 27-44

Online ISSN: 3041-9018

Journal of Green Energy Research and Innovation

Journal Homepage: www.jgeri.araku.ac.ir

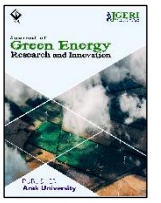

Introducing New Control Methods to Apply in Flexible Photovoltaic Systems at the 3-Phase 4-Wire Grids

Saeid Khani [1], Leila Mohammadian [2,*]

[1] *East Azarbaijan Electric Power Distribution Company, Tabriz, Iran.*

[2] *Department of Electrical Engineering, Shab.C., Islamic Azad University, Shabestar, Iran.*

A R T I C L E I N F O

Keywords:
Active Filter,
Corrected P-Q Theory,
Enhanced Vectorial Theory,
Flexible Photovoltaic System.

Article History:
Received: 15 April 2025;
Revised: 25 May 2025;
Accepted: 30 June 2025.

Article type:
Research Article

* ***Corresponding authors***
E-mail address
Le.mohammadian@iau.ac.ir (L. Mohammadian)

A B S T R A C T

Integrating photovoltaic (PV) generation with active filtering (AF) in three-phase four-wire distribution networks enhances power quality while maximizing renewable energy utilization. This study presents two advanced control strategies—the corrected p-q theory and the enhanced vectorial control method—to optimize system performance under unbalanced and distorted grid conditions. The corrected p-q strategy ensures harmonic compensation, reactive power balance, and neutral current elimination, stabilizing DC-link voltage with THD levels below 3%. Meanwhile, the enhanced vectorial control approach provides superior harmonic suppression, reducing THD to 0.88% and neutral current RMS to 0.035, while maintaining DC-link voltage at a stable level, optimizing energy storage and power conversion. Both strategies are validated through PSCAD/EMTDC simulations, demonstrating their adaptability in dynamically adjusting PV power injection in response to irradiance and temperature variations. The MPPT algorithm effectively tracks optimal power points, ensuring efficient grid interaction and power stabilization. A comparative analysis confirms the enhanced vectorial control method's advantages in harmonic reduction and reactive power compensation, making it preferable for stringent grid applications while reinforcing the role of PV systems as intelligent multi-functional energy units.

1. Introduction

The global energy demand has increased significantly in recent years, requiring advanced power management strategies to ensure grid stability and efficiency. As of today, approximately 75% of global energy consumption relies on fossil fuels, leading to environmental pollution, climate change, and diminishing natural resources [1]. Given these challenges, renewable energy sources, particularly PV systems, have emerged as sustainable alternatives for electricity generation [2].

However, integrating PV systems into modern power grids presents significant challenges due to power quality issues introduced by nonlinear loads such as industrial converters, rectifiers, and EV chargers, leading to harmonic distortions, excessive reactive power demand, and voltage instability [3]. To address these challenges, Active Power Filters (APFs) have been widely adopted to mitigate harmonic contamination, ensuring IEEE-519 standard compliance [4]. Nonetheless, standalone APFs require additional infrastructure investment, limiting their implementation in large-scale power networks [5].

Flexible Photovoltaic (FPV) systems provide an innovative solution by merging PV generation with active filtering capabilities, thereby improving power quality while maintaining energy efficiency. Several studies have explored methods for optimizing FPV systems: Reference [6] investigated the impact of harmonic pollution in distributed networks, proposing optimal capacitor placement to enhance voltage stability and reactive power compensation. Reference [7] explored hybrid AC/DC microgrid architectures, introducing collaborative control mechanisms for harmonic suppression and improved voltage regulation. Authors of [8] proposed a multi-functional PV inverter designed to enhance grid resilience by compensating reactive power and balancing harmonic distortions.

Literature [9] applied machine learning-based controllers to optimize harmonic mitigation and voltage stability, reinforcing the adaptability of PV systems in smart grids. Reference [10] developed fuzzy logic controllers to improve active harmonic filtering, ensuring PV systems remain efficient in dynamically changing grid environments. Paper [11] designed a universal PV-integrated active filter, demonstrating its capability to enhance energy management and grid stability under various operational conditions. Paper [12] investigated smart inverter control methods, emphasizing the need for coordinated reactive power control to prevent voltage violations. Reference [13] studied fault detection and diagnosis techniques for grid-connected PV systems, particularly under irradiance variations, providing insights into stabilizing PV performance under diverse environmental conditions. Paper [14] examined the integration of distributed PV sources into smart grids, offering a comprehensive analysis of the challenges associated with network reliability and operational efficiency. Authors of [15] reviewed vectorial control applications for PV-AF systems, highlighting their advantages in load compensation and harmonic suppression under unbalanced and distorted supply voltages. Reference [16] conducted a broad literature review of control techniques in PV systems, reinforcing the importance of adaptive algorithms for MPPT optimization and power regulation. Literature [17] explored advanced flexible control technologies, showcasing their role in improving PV energy storage integration and network stabilization. Reference [18] investigated emerging trends in grid-connected PV systems, particularly for ancillary services and real-time voltage control strategies. Literature [19] compared harmonic analysis methods for high-voltage vs. medium-voltage PV integration, highlighting their effects on overall system efficiency and stability. Paper [20] introduced a meta-heuristic algorithm-based hybrid power filter, optimizing power flow regulation for improved harmonic compensation in smart grids. Paper [21] discussed grid-friendly power control mechanisms, presenting an adaptive approach for smart PV system operation and voltage control in distributed networks. Despite these technological advancements, FPV systems still face two major challenges that must be addressed:

Maximum Power Point Tracking (MPPT): Maintaining optimal energy extraction under fluctuating irradiance and dynamic load variations.

Reference Current Calculation in Three-Phase Four-Wire Systems: Ensuring accurate harmonic suppression and neutral current elimination, especially under non-sinusoidal and unbalanced supply conditions.

To address these challenges, this study presents two advanced control strategies tailored for FPV systems operating as both an active filter and a power source:

Corrected p-q Theory: An improved formulation of instantaneous power theory, allowing harmonic compensation, reactive power regulation, and DC-link voltage stabilization while ensuring adaptability in PV power injection.

Enhanced Vectorial Control: A grid-compatible compensation technique that ensures balanced sinusoidal source currents, null reactive power, and neutral current suppression, while maintaining high power quality and stable DC-link voltage.

The remainder of this paper is structured as follows:

Section 2 provides a detailed FPV system architecture description, introducing the corrected p-q control strategy.

Section 3 presents the enhanced vectorial control methodology, discussing its theoretical foundation, and reports PSCAD/EMTDC simulation results, assessing system performance under diverse operational scenarios.

Section 4 compares the two control strategies, focusing on harmonic suppression, MPPT efficiency, power regulation, and neutral current elimination, and finally, a comparison between the proposed control methods with other methods in the referenced literature is confirmed.

Section 5 concludes the study, discussing key findings, practical implications, and future research directions.

A graphical abstract summarizing the research workflow, key objectives, and contributions is provided in Figure 1.

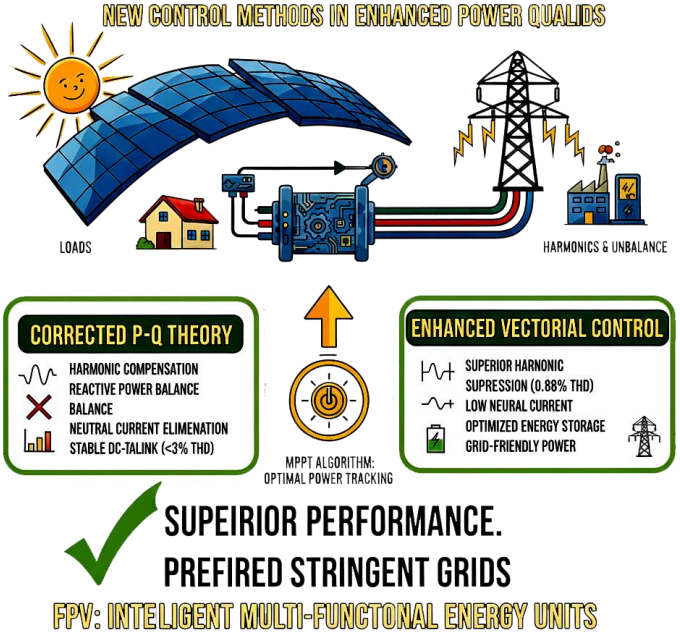

Figure 1. Graphical abstract.

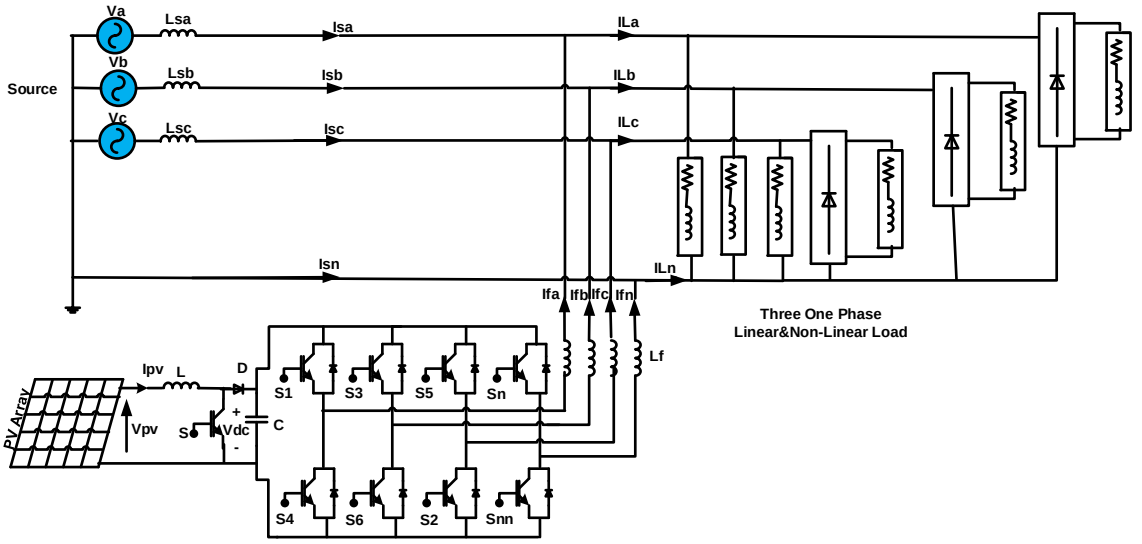

Figure 2. Structure of the FPV system.

2. System Description and the Proposed Corrected p-q Control Strategy

As shown in Figure 2, the FPV system comprises a PV array, a boost converter, and a three-phase four-leg inverter connected to an unbalanced and distorted utility grid. This grid supplies three single-phase linear and nonlinear unbalanced loads. The FPV system employs a corrected p-q control strategy and a simplified MPPT method to inject the maximum available power from the PV array into the grid while compensating for imbalances.

The FPV system uses a three-phase, four-leg inverter to deal with issues such as phase imbalance, harmonic distortion in the load current, reactive power demand, and neutral-line current. An additional DC–DC boost stage performs MPPT. When solar production is low and the PV array cannot deliver the required active power, the AC grid supplies the load directly, while the PV unit contributes only the compensating current needed to cancel the unwanted components created by the nonlinear three-phase load. Under normal conditions, the PV subsystem provides the bulk of the active power for both the load and the grid, allowing the system to operate similarly to a UPS.

A modified p–q approach is used to design the control scheme. This framework regulates the switching pulses for both the boost converter and the inverter based on measurements of the line currents (I_{La}, I_{Lb}, I_{Lc}), phase voltages (u_a, u_b, u_c), dc link voltage (V_{dc}), current and voltage of PV system (I_{PV}, V_{PV}).

2.1. The Proposed Corrected p-q Control Theory

The instantaneous reactive power theory was introduced in the early 1980s as an effective control strategy for mitigating the impact of three-phase nonlinear loads using an APF. The initial p-q theory was developed for three-phase three-wire systems, assuming balanced and sinusoidal supply voltages. The fundamental principle of this theory is based on coordinate transformation, converting the phase reference system into the 0-α-β reference frame, thereby facilitating the separation of active and reactive power components for precise control and compensation [13,14].

Throughout this paper, the following notational conventions are adopted:

- Lowercase variables represent instantaneous values.
- Uppercase variables denote average values (steady-state components).
- Lowercase variables with a tilde (~) indicate oscillatory components.
- Subscript 'L' refers to load requirements.
- Subscript 'C' corresponds to compensator supply (APF output).
- Subscript 'S' designates source supply (grid-side power).

$$\vec{u} = [u_a \quad u_b \quad u_c]^t \tag{1}$$

$$\vec{i}_L = \begin{bmatrix} i_{La} & i_{Lb} & i_{Lc} \end{bmatrix}^t \tag{2}$$

The Clarke transformation (also known as the α-β transformation) is used to convert three-phase system voltages and currents from the a-b-c reference frame (given in Equations (1) and (2)) to the 0-α-β reference frame, facilitating analysis and control in instantaneous power theory and harmonic compensation applications. The transformation equations are defined as Equations (3) and (4).

$$\begin{bmatrix} e_0 \\ e_\alpha \\ e_\beta \end{bmatrix} = \sqrt{\frac{2}{3}} \begin{bmatrix} \frac{1}{\sqrt{2}} & \frac{1}{\sqrt{2}} & \frac{1}{\sqrt{2}} \\ 1 & -\frac{1}{2} & -\frac{1}{2} \\ 0 & \frac{\sqrt{3}}{2} & -\frac{\sqrt{3}}{2} \end{bmatrix} \begin{bmatrix} u_a \\ u_b \\ u_c \end{bmatrix} \tag{3}$$

$$\begin{bmatrix} i_{L0} \\ i_{L\alpha} \\ i_{L\beta} \end{bmatrix} = \sqrt{\frac{2}{3}} \begin{bmatrix} \frac{1}{\sqrt{2}} & \frac{1}{\sqrt{2}} & \frac{1}{\sqrt{2}} \\ 1 & -\frac{1}{2} & -\frac{1}{2} \\ 0 & \frac{\sqrt{3}}{2} & -\frac{\sqrt{3}}{2} \end{bmatrix} \begin{bmatrix} i_{La} \\ i_{Lb} \\ i_{Lc} \end{bmatrix} \tag{4}$$

In the transformed 0-α-β coordinate system, the various power terms associated with the load can be defined based on the instantaneous p-q theory. These terms distinguish between active, reactive, and oscillatory power components, enabling precise control and compensation in three-phase four-wire systems (refer to Equation (5)).

$$\begin{aligned} p_{L0}(t) &= e_0 i_{L0} = p_{L0} + \overline{P}_{L0} \\ p_{L\alpha\beta}(t) &= \begin{bmatrix} e_\alpha & e_\beta \end{bmatrix} \begin{bmatrix} i_{L\alpha} \\ i_{L\beta} \end{bmatrix} = p_{L\alpha\beta} + \overline{P}_{L\alpha\beta} \\ \vec{q}_{L\alpha\beta}(t) &= \begin{bmatrix} e_\alpha & e_\beta \end{bmatrix}^T \times \begin{bmatrix} i_{L\alpha} & i_{L\beta} \end{bmatrix}^T \end{aligned} \tag{5}$$

In the vectorial representation of the instantaneous p-q theory, the voltage space vectors can be defined to enhance power control analysis. The three voltage space vectors are given by Equation (6) and are shown in Figure 3.

$$\vec{e}_0 = \begin{bmatrix} e_0 \\ 0 \\ 0 \end{bmatrix}, \ \vec{e}_{\alpha\beta} = \begin{bmatrix} 0 \\ e_\alpha \\ e_\beta \end{bmatrix}, \ \vec{e}_{-\beta\alpha} = \begin{bmatrix} 0 \\ -e_\beta \\ e_\alpha \end{bmatrix} \tag{6}$$

In the 0-α-β reference frame, the load current vector can be expressed using Clarke transformation principles. This formulation facilitates instantaneous power analysis and harmonic compensation in three-phase systems. The vector representation is given by Equation (7):

$$\vec{i}_L = \frac{p_{L\alpha\beta}(t)}{e_{\alpha\beta}^2} \vec{e}_{\alpha\beta} + \frac{p_{L0}(t)}{e_0^2} \vec{e}_0 + \frac{q_{L\alpha\beta}(t)}{e_{\alpha\beta}^2} \vec{e}_{-\beta\alpha} \tag{7}$$

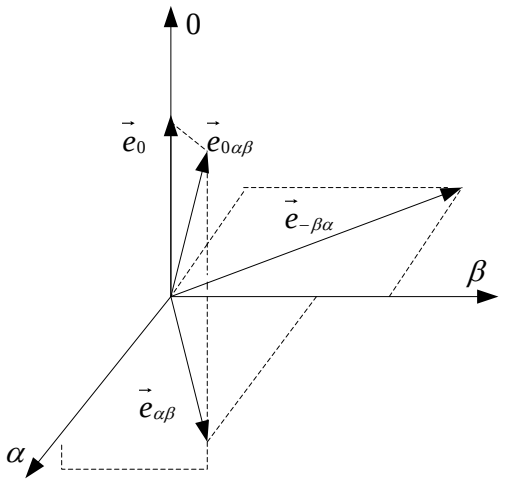

Figure 3. New voltage vectors in 0- α - β coordinates system.

In the sinusoidal source current compensation objective of p-q theory, the goal is to achieve a sinusoidal and balanced source current, ensuring it remains in phase with the supply voltage under ideal conditions. When the voltage is sinusoidal and balanced, the source current aligns precisely with it. However, in cases where the voltage exhibits distortions or unbalanced components, the source current must still align with the positive-sequence fundamental element of the voltage to maintain grid stability. This condition must be satisfied regardless of supply voltage variations and load characteristics, ensuring adequate compensation across different operating scenarios. Consequently, after implementing harmonic mitigation and reactive power compensation, the source current can be mathematically represented as Equation (8):

$$\vec{i}_S = G_e \vec{e}^{+}_{\alpha\beta 1} \tag{8}$$

The instantaneous power balance in a system involving a source, load, and compensator can be expressed as Equation (9):

$$p_C(t) = p_L(t) - p_S(t) \tag{9}$$

Then, substituting Equation (8) in Equation (9), Equation (10) is given:

$$p_C(t) = p_L(t) - \vec{e}_{\alpha\beta} G_e \vec{e}^{+}_{\alpha\beta 1} \tag{10}$$

In the conventional p-q theory, the compensator's average power is considered zero. However, in the corrected p-q theory, a nonzero compensator power, $P_{PV} - P_{cap}$, is introduced to ensure DC-link voltage stability at its reference value while simultaneously enabling PV power injection into the grid. Consequently, the proportionality constant is derived as Equation (11).

$$\frac{1}{T}\int_T p_C(t) = \frac{1}{T}\int_T p_L(t) - \frac{1}{T}\int_T \vec{e}_{\alpha\beta} G_e \vec{e}^{+}_{\alpha\beta 1} = P_{PV} - P_{cap} \tag{11}$$

$$\frac{1}{T}\int_T p_L(t) - P_{PV} + P_{cap} = \frac{1}{T}\int_T \vec{e}_{\alpha\beta} G_e \vec{e}^{+}_{\alpha\beta 1}$$

$$G_e = \frac{\overline{P}_{L\alpha\beta} - P_{PV} + P_{cap}}{E_1^{+2}}$$

Where E_1^{+2} represents the square of the RMS value of the positive-sequence fundamental component of the voltage. This term is crucial in determining the proportionality constant required for ensuring DC-link voltage regulation and simultaneous PV power injection into the grid, as established in the corrected p-q theory formulation (refer to Equation (12)).

$$E_1^{+2} = \frac{1}{T}\int_T (e_{\alpha 1}^{+2} + e_{\beta 1}^{+2}) dt \tag{12}$$

Hence, after compensation, the source's current expression will be as Equation (13):

$$\vec{i}_S = \frac{\overline{P}_{L\alpha\beta} - P_{PV} + P_{cap}}{E_1^{+2}} \vec{e}^{+}_{\alpha\beta 1} \tag{13}$$

Thus, from Equations (7) and (13), the compensation current is calculated as Equation (14).

$$\vec{i}_C = \vec{i}_L - \vec{i}_S = \frac{p_{L\alpha\beta}(t)}{e_{\alpha\beta}^2}\vec{e}_{\alpha\beta} + \frac{p_{L0}(t)}{e_0^2}\vec{e}_0 + \frac{q_{L\alpha\beta}(t)}{e_{\alpha\beta}^2}\vec{e}_{-\beta\alpha} - \frac{\overline{P}_{L\alpha\beta} - P_{PV} + P_{cap}}{E_1^{+2}}\vec{e}^{+}_{\alpha\beta 1} \tag{14}$$

Therefore, different power terms of the compensator are defined in Equation (15).

$$\begin{aligned} p_{C0}(t) &= \vec{e}_0 . \vec{i}_C = p_{L0}(t) \\ p_{C\alpha\beta}(t) &= \vec{e}_{\alpha\beta} . \vec{i}_C = p_{L\alpha\beta}(t) - \frac{\overline{P}_{L\alpha\beta} - P_{PV} + P_{cap}}{E_1^{+2}}(e_\alpha e_{\alpha 1}^{+} + e_\beta e_{\beta 1}^{+}) \\ q_{C\alpha\beta}(t) &= \vec{e}_{-\beta\alpha} . \vec{i}_C = q_{L\alpha\beta}(t) - \frac{\overline{P}_{L\alpha\beta} - P_{PV} + P_{cap}}{E_1^{+2}}(e_\alpha e_{\beta 1}^{+} - e_\beta e_{\alpha 1}^{+}) \end{aligned} \tag{15}$$

In the mapping matrices format, the control strategy may be expressed as Equation (16).

$$\begin{bmatrix} i_{0,ref} \\ i_{\alpha,ref} \\ i_{\beta,ref} \end{bmatrix} = \frac{1}{e_0 e_{\alpha\beta}^2} \begin{bmatrix} e_{\alpha\beta}^2 & 0 & 0 \\ 0 & e_0 e_\alpha & -e_0 e_\beta \\ 0 & e_0 e_\beta & e_0 e_\alpha \end{bmatrix} \times \begin{bmatrix} p_{L0}(t) \\ p_{L\alpha\beta}(t) - \dfrac{\overline{P}_{L\alpha\beta} - P_{PV} + P_{cap}}{E_1^{+2}} (e_\alpha e_{\alpha 1}^{+} + e_\beta e_{\beta 1}^{+}) \\ q_{L\alpha\beta}(t) - \dfrac{\overline{P}_{L\alpha\beta} - P_{PV} + P_{cap}}{E_1^{+2}} (e_\alpha e_{\beta 1}^{+} - e_\beta e_{\alpha 1}^{+}) \end{bmatrix} \tag{16}$$

Eventually, Equation (17) provides the reference currents in *abcn* reference frame.

$$\begin{bmatrix} i_{a,ref} \\ i_{b,ref} \\ i_{c,ref} \end{bmatrix} = \frac{\sqrt{2}}{3} \begin{bmatrix} \frac{1}{2\sqrt{2}} & 1 & 0 \\ \frac{1}{2\sqrt{2}} & -\frac{1}{2} & \frac{\sqrt{3}}{2} \\ \frac{1}{2\sqrt{2}} & -\frac{1}{2} & -\frac{\sqrt{3}}{3} \end{bmatrix} \begin{bmatrix} i_{0,ref} \\ i_{\alpha,ref} \\ i_{\beta,ref} \end{bmatrix} \tag{17}$$

$$i_{n,ref} = i_{a,ref} + i_{b,ref} + i_{c,ref}$$

These reference currents enable the PV array to deliver its maximum extractable power to the grid while simultaneously correcting current imbalance, suppressing load-current harmonics, supplying the load's reactive power requirement, and canceling the neutral-line current.

2.2. *MPPT Control Theory*

The PV array power curve exhibits a zero slope at the MPP, a positive slope on the side before the MPP, and a negative slope beyond the MPP, as indicated in Equation (18).

$$\begin{cases} \dfrac{dP}{dV} = 0 & at\ MPP \\ \dfrac{dP}{dV} > 0 & left\ of\ \ MPP \\ \dfrac{dP}{dV} < 0 & right\ of\ \ MPP \end{cases} \tag{18}$$

A straightforward proportional-integral (PI) controller can be used to maintain $dP/dV = 0$. The PI controller's output determines the duty cycle (D) of the boost converter. The block diagram illustrating this approach is presented in Figure 4. Using Equations (17) and (18) as a basis, the proposed control scheme is developed and depicted in Figure 5.

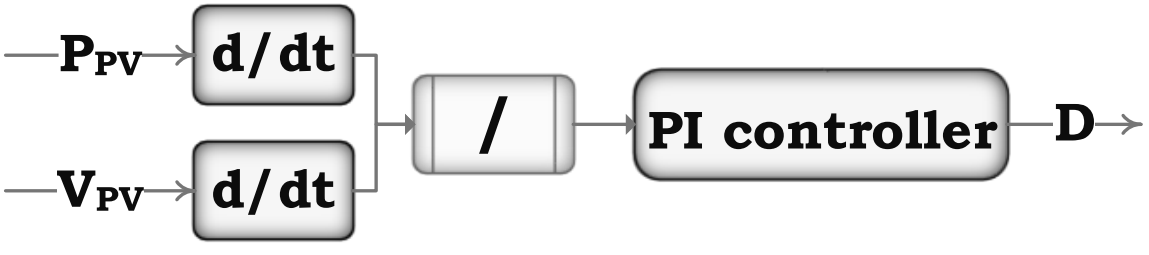

Figure 4. A simple MPPT algorithm.

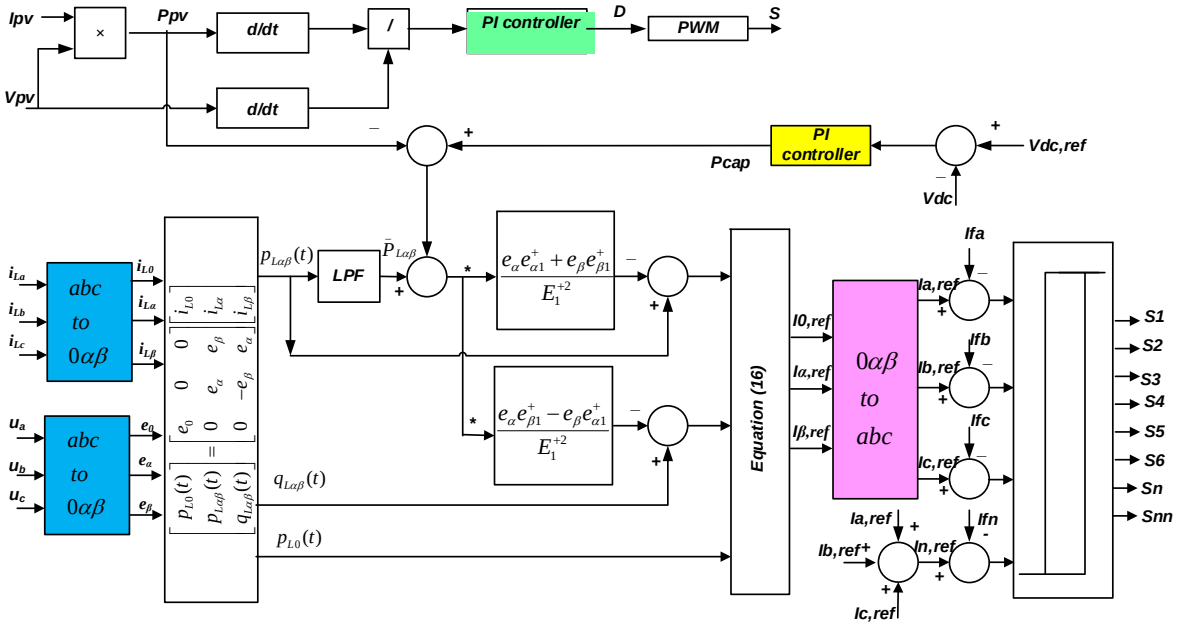

Figure 5. Block diagram of the system controller.

2.3. *Simulation Report of the Suggested Corrected p-q Control Strategy*

To validate the proposed corrected p-q control strategy for the FPV system connected to a three-phase four-wire network, a detailed simulation study was performed using PSCAD/EMTDC software. To assess the system's response to variations in PV power, three operational scenarios were considered, reflecting changes in irradiance and temperature. Figure 6 illustrates these three stages. In the first stage (0–0.1 s), the irradiance is approximately 800 W/m^2 and the temperature is 40°C. The second stage begins when the temperature drops to 15°C while irradiance remains constant, lasting until 0.175 s. The third stage, from 0.175 s to 0.25 s, assumes irradiance falls to 0 W/m^2, temperature remains steady, and the FPV real power output is zero.

Figure 7(a) shows the supply voltages in all scenarios, given by:

- $U_a = 254.55\sin(2\pi \cdot 60t) + 25.45\sin(2\pi \cdot 300t) + 17.67\sin(2\pi \cdot 420t)$
- $U_b = 311\sin(2\pi \cdot 60t - 120°) + 31.1\sin(2\pi \cdot 300t + 120°) + 21.21\sin(2\pi \cdot 420t - 120°)$
- $U_c = 353.55\sin(2\pi \cdot 60t + 120°) + 35.35\sin(2\pi \cdot 300t - 120°) + 24\sin(2\pi \cdot 420t + 120°)$

The neutral line current and load currents are depicted in Figure 7(b). Table 1 lists the power system parameters applied in the simulations.

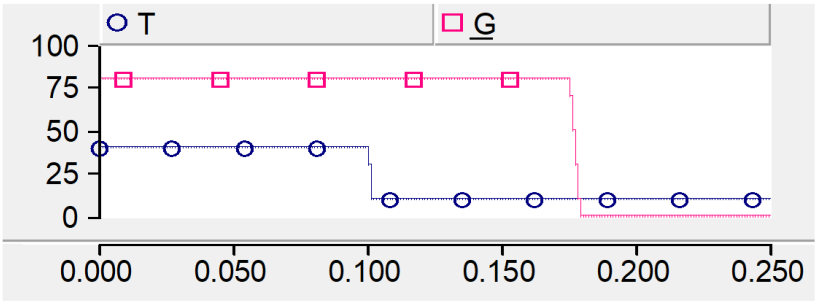

Figure 6. Diagram of variation in light intensity and temperature.

Table 1. Simulation Parameters.

$L_f = 10$ mH	VLL,rms = 380 v
$L_{dc} = 26$ mH	fs = 60 Hz
$C_{dc} = 650$ µF	Vdc,ref = 800 v
$f_{boost} = 3500$ Hz	Linear balanced and unbalanced load = 1.5 kW, 2 kVAR

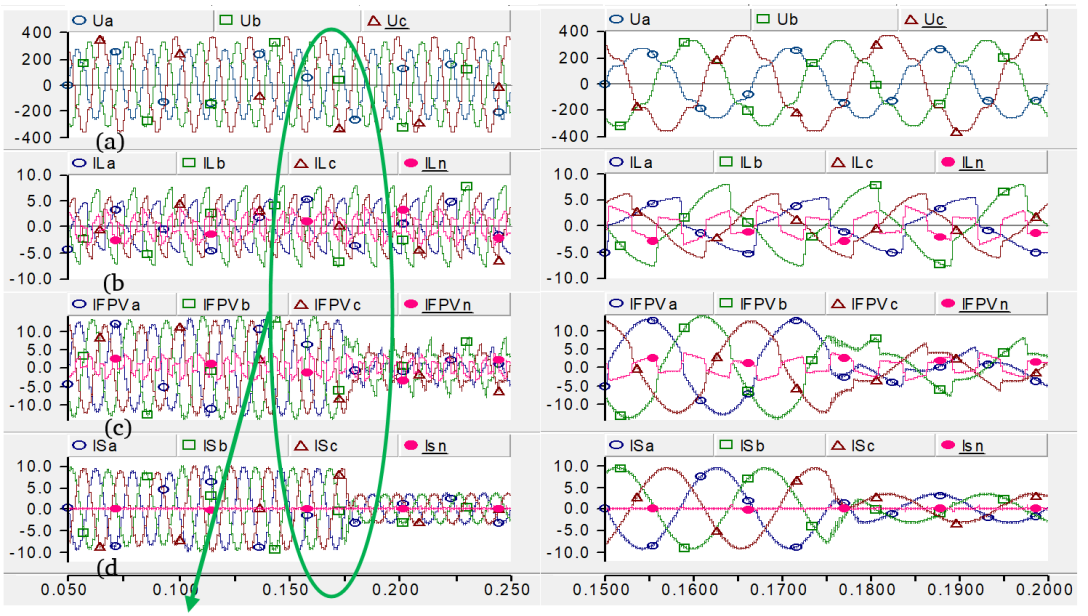

Figure 7. Simulation results: (a) Grid Voltage, (b) unbalanced load currents, (c) FPV currents, (d) Grid Currents.

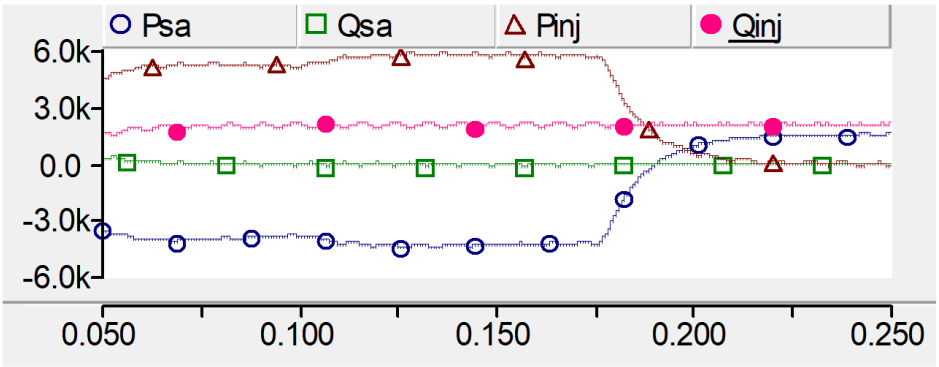

Figure 8. The Source and FPV active and reactive injected power.

Table 2. THD Values.

THD(%) Stage	i_{sa}	i_{sb}	i_{sc}
Before compensation	30.3	20.52	16.73
After compensation ($P_{inj}=0$ kw)	3	2.45	2.81
After compensation ($P_{inj}=5$kw)	1.16	1.26	1.3
After compensation ($P_{inj}=5.8$kw)	1.1	1.21	1

Figure 7 presents the simulation outcomes for the three operational stages, demonstrating the FPV system's capability to operate simultaneously as an active power filter (APF) and a power supplier, or solely as an APF, under unbalanced and non-sinusoidal voltage conditions. The green circle highlights the moment when grid disturbances occur, with a zoomed-in view on the right side of the figure to clearly depict these disturbances. As shown in Figure 7(d), the FPV system effectively compensates for current unbalance, load current harmonics, load reactive power, and neutral line current. Across all stages, the total harmonic distortion (THD) remains below 3%, and the RMS value of the neutral current is 0.09 A. Detailed THD values for source currents under all scenarios are provided in Table 2. Figure 8 displays the active and reactive power injected by both the source and the FPV system, indicating that the PV array supplies the entire reactive power demanded by the load.

Moreover, Figure 9 illustrates the DC-link voltage of the capacitor for these three stages. As illustrated, the capacitor voltage is stabilized at 800V, which is approximately twice the magnitude of the line voltage (380V), ensuring efficient energy management and system performance.

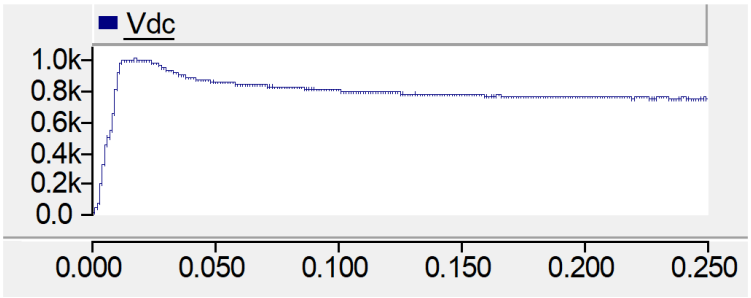

Figure 9. The DC-Link Voltage.

2.4. Results Analysis of the Proposed Corrected p-q Control Theory

In the previous section, the corrected p-q control theory was applied to a Flexible Photovoltaic (FPV) system integrated into a three-phase four-wire distribution grid, accounting for both unbalanced linear and nonlinear loads, as well as a distorted and unbalanced voltage supply. Applying this control strategy compensates for current unbalance, suppression of load current harmonics, fulfillment of reactive power demand, and neutral current mitigation. Consequently, the source current became balanced and sinusoidal, with a unity power factor achieved under all operational conditions. Simulation results illustrate the performance of the FPV system across various PV operational conditions. During the first two stages, the FPV system injects real power generated from the PV array into the grid and functions as an APF, ensuring enhanced power quality. In the third stage, the FPV system operates solely as an APF, with no power injection from the PV source. Across all three operating scenarios, PV power injection is different, and the THD is calculated for each condition.

The results demonstrate that the proposed control strategy effectively compensates for current unbalance, suppresses load current harmonics, meets reactive power demand, and eliminates neutral current fluctuations, reinforcing its applicability for power quality enhancement in renewable energy-integrated distribution networks.

3. System Description and the Proposed Enhanced Vectorial Control Strategy

3.1. System Description

The circuit block diagram of the grid-connected PV system is shown in Figure 10. As shown in the figure, the whole 4-wire system is composed of a PV array, a Boost converter, a three-phase inverter, a three-phase balanced, linear, and non-linear load, and the unbalanced and harmonic utility grid. The proposed scheme employs a vectorial theory-controlled three-phase 4-leg inverter to perform reactive power compensation, harmonic elimination, and to inject the maximum power of the PV array into the grid. A DC/DC voltage boost converter is used to address the MPPT. Under poor generation conditions of the PV system, the AC source supplies the active power to the load directly, and the PV system only injects the compensating current to eliminate the undesired current components generated by a three-phase nonlinear load. In the normal mode, the PV system mainly provides active power to the load and utility; in other words, it acts as an uninterruptible power supply. The vectorial theory is applied to design the control system, which provides pulse gates of the Boost switches and inverter switches by measuring the line currents (I_{La}, I_{Lb}, I_{Lc}), phase voltages (*Va*, *Vb*, *Vc*), dc link voltage (*Vdc*), current and voltage of the PV system (*Ipv*, *Vpv*).

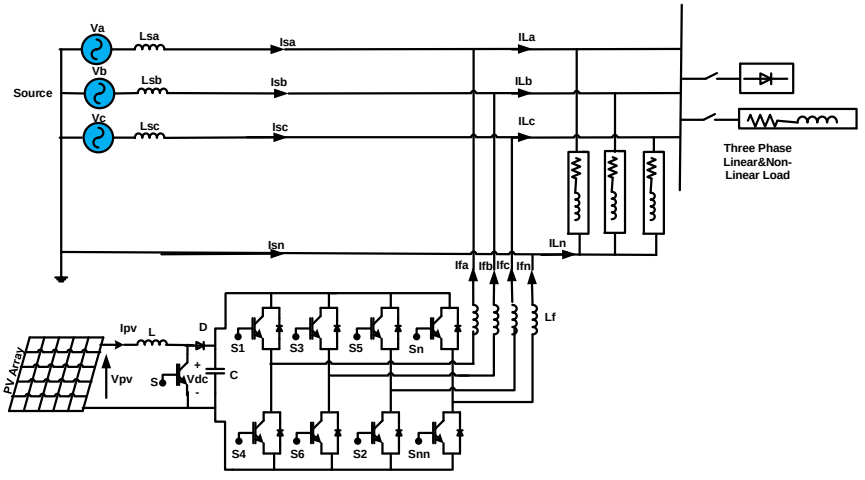

Figure 10. The whole structure of the three-phase 4-wire grid-connected PV power system.

3.2. The Proposed Enhanced Vectorial Control Strategy

In the early 1980s, the instantaneous reactive power theory was developed to provide an effective control approach for compensating three-phase nonlinear loads via APFs [11]. Its original form, the p-q theory, was intended for three-phase, three-wire nonlinear systems under balanced conditions with sinusoidal voltage sources. This strategy successfully ensured that, after compensation, the source currents remained sinusoidal and closely followed the supply voltage waveform. Over the years, various modifications and alternative formulations have been proposed, enhancing and refining the original p-q theory. These include:

- The Park transformation (d-q coordinates),
- The corrected or cross-product theory,
- The p-q-r theory, a novel extension of the original approach,
- The vectorial theory offers an advanced perspective on power compensation.

In the following section, an enhanced vectorial theory, applied to achieve the stated control objectives, is explored in detail.

Voltage and current phase vectors are represented by Equations (19) and (20).

$$\vec{u} = \begin{bmatrix} u_a & u_b & u_c \end{bmatrix}^t \tag{19}$$

$$\vec{i} = \begin{bmatrix} i_a & i_b & i_c \end{bmatrix}^t \tag{20}$$

The zero-sequence phase voltage vector is defined as Equation (21).

$$\vec{v}_0 = \begin{bmatrix} v_0 & v_0 & v_0 \end{bmatrix}^t$$

$$v_0 = \frac{u_a + u_b + u_c}{3} \tag{21}$$

Thus, the voltage vector $\vec{v}$ is provided as Equation (22).

$$\vec{v} = \vec{u} - \vec{v}_0 \tag{22}$$

Unlike the other formulations discussed, the vectorial theory does not require any coordinate transformations. It retains the original power variables to define instantaneous active power without the zero-sequence component $p(t)$, instantaneous zero-sequence power $p_0(t)$, and instantaneous imaginary power $q(t)$directly in the phase coordinates, as expressed in Equations (23)–(25).

$$p(t) = \vec{v}.\vec{i} = v_a i_a + v_b i_b + v_c i_c \tag{23}$$

$$p_0(t) = \vec{v_0}.\vec{i} = v_0 i_a + v_0 i_b + v_0 i_c \tag{24}$$

$$\vec{q}(t) = \vec{v} \times \vec{i} = \begin{bmatrix} v_a \\ v_b \\ v_c \end{bmatrix} \times \begin{bmatrix} i_a \\ i_b \\ i_c \end{bmatrix} = \begin{bmatrix} v_a i_c - v_c i_b \\ v_c i_a - v_a i_c \\ v_a i_b - v_b i_a \end{bmatrix} \tag{25}$$

Equation (26) determines the currents concerning the three power variables.

$$\begin{bmatrix} i_a \\ i_b \\ i_c \end{bmatrix} = \frac{p}{v^2} \begin{bmatrix} v_a \\ v_b \\ v_c \end{bmatrix} + \frac{p_0}{v_0^2} \begin{bmatrix} v_0 \\ v_0 \\ v_0 \end{bmatrix} + \frac{1}{\sqrt{3}} \frac{\left|\vec{q}(t)\right|}{v^2} \begin{bmatrix} v_b - v_c \\ v_c - v_a \\ v_a - v_b \end{bmatrix} \tag{26}$$

Considering the constant source power as a compensation objective and unbalanced and non-sinusoidal supply voltage, the compensation current in vectorial theory is achieved as Equation (27).

$$\begin{bmatrix} i_{ca} \\ i_{cb} \\ i_{cc} \end{bmatrix} = \begin{bmatrix} i_{La} \\ i_{Lb} \\ i_{Lc} \end{bmatrix} - \frac{P_{Lu}}{U_1^{+2}} \begin{bmatrix} u_{a1}^+ \\ u_{b1}^+ \\ u_{c1}^+ \end{bmatrix} \tag{27}$$

u_{a1}^+, u_{b1}^+ and u_{c1}^+ are the voltage-positive sequence fundamental components of each phase, and U_1^{+2} show the RMS value of the voltage's positive sequence fundamental component as given by Equation (28).

$$U_1^{+2} = \frac{1}{T}\int_T (u_{a1}^{+2} + u_{b1}^{+2} + u_{c1}^{+2})dt \tag{28}$$

Moreover, P_{Lu} is time average value of the load's instantaneous real power as defined by Equation (29).

$$p_{Lu}(t) = \vec{u}.\vec{i} = u_a i_a + u_b i_b + u_c i_c = \tilde{p}_{Lu} + P_{Lu} \tag{29}$$

To enable injection of instantaneous PV power, a DC term $P_{pv}$is incorporated into Equation (9). Similarly, an additional term $P_{cap}$is included to control the capacitor voltage [10]. Consequently, the overall reference currents are determined as shown in Equation (30).

$$\begin{bmatrix} i_{a,ref} \\ i_{b,ref} \\ i_{c,ref} \end{bmatrix} = \frac{p_L}{v^2}\begin{bmatrix} v_a \\ v_b \\ v_c \end{bmatrix} - \frac{P}{U_1^{+2}}\begin{bmatrix} u_{a1}^{+} \\ u_{b1}^{+} \\ u_{c1}^{+} \end{bmatrix} + \frac{p_{L0}}{v_0^2}\begin{bmatrix} v_0 \\ v_0 \\ v_0 \end{bmatrix} + \frac{1}{\sqrt{3}}\frac{|q_L|}{v^2}\begin{bmatrix} v_b - v_c \\ v_c - v_a \\ v_a - v_b \end{bmatrix}$$
$$P = P_{Lu} + P_{cap} - P_{pv} \tag{30}$$

Based on Equation (30), the control system is designed as in Figure 11.

3.3. *Simulation Results for the Proposed Enhanced Vectorial Control Strategy*

In this section, the simulations for this study were conducted using PSCAD/EMTDC. The FPV model was designed to operate under three distinct environmental conditions:

1. Standard PV operation (800 W/m^2, 40°C) – tracking optimal MPPT while providing active filtering.
2. Reduced temperature condition (15°C, constant irradiance) – testing adaptability to dynamic conditions.
3. Zero irradiance scenario (0 W/m^2, constant temperature) – evaluating system performance when PV generation ceases, operating solely as an APF.
4. Key system parameters included:

- DC-link voltage: 1200V (maintaining stability under load fluctuations).
- Total Harmonic Distortion (THD): Below 1%, demonstrating compliance with IEEE standards.
- Compensation Efficiency: Neutral current reduced to 0.035 RMS, proving effective load balancing.

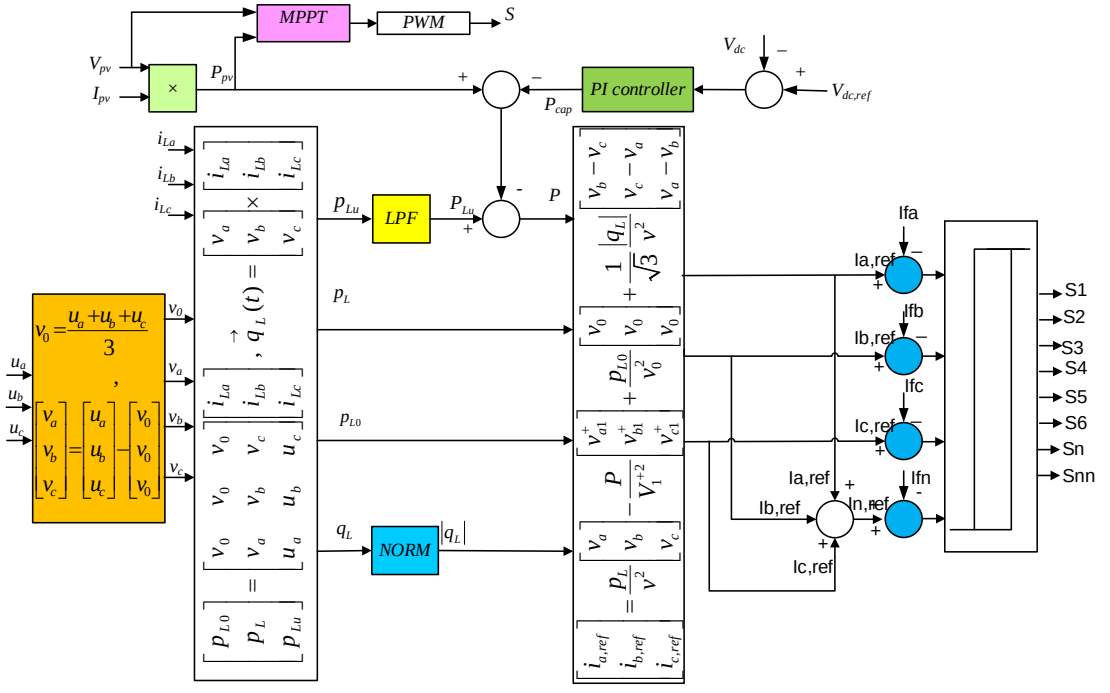

Figure 11. The system controller block diagram based on vectorial theory.

The system was analyzed under four different PV power injection conditions. In the first simulation, the PV system's injection was neglected, evaluating its operation solely as an active filter under unbalanced and non-sinusoidal voltage supply. In the subsequent simulations, the performance of the proposed system in tracking the PV array's maximum power point (MPP) while compensating for nonlinear and unbalanced load currents across varying PV conditions was examined. The supply voltages and load currents are as follows (Figures 12 and 13):

- **Ua:** $254.55 \sin(2\pi \times 60t) + 25.45 \sin(2\pi \times 300t) + 17.67 \sin(2\pi \times 420t)$
- **Ub:** $311 \sin(2\pi \times 60t - 120) + 31.1 \sin(2\pi \times 300t + 120) + 21.21 \sin(2\pi \times 420t - 120)$
- **Uc:** $353.55 \sin(2\pi \times 60t + 120) + 35.35 \sin(2\pi \times 300t - 120) + 24 \sin(2\pi \times 420t + 120)$

The resulting neutral line current is illustrated in Figure 13(b). Power system parameters used for the simulations are summarized in Table 3.

Table 3. Parameters of the simulated power system.

$L_f = 10$ mH	$V_{LL,rms} = 380$ v
$C_f = 1$ μF	$f_s = 60$ Hz
$L_{dc} = 300$ mH	$V_{dc,ref} = 1200$ v
$C_{dc} = 600$ μF	Linear balanced and unbalanced load = 1.7 kW, 1.7 kVAR
$f_{boost} = 3500$ Hz	Non-linear load = 14.6 kW, 6 kVAR

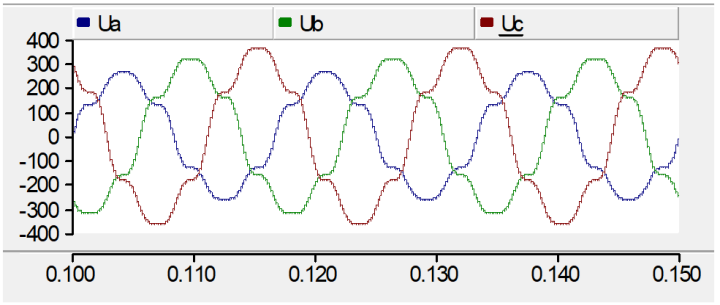

Figure. 12. Three-phase unbalanced and non-sinusoidal voltage supply.

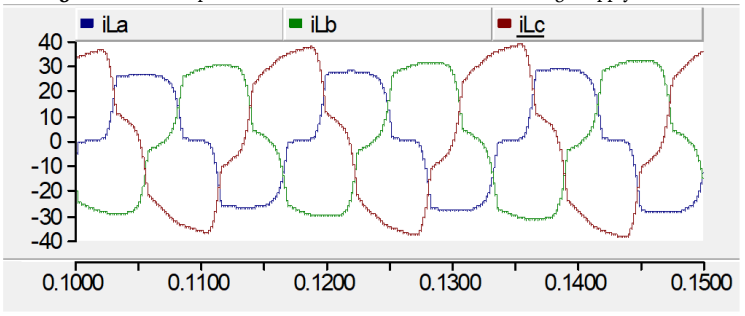

(a)

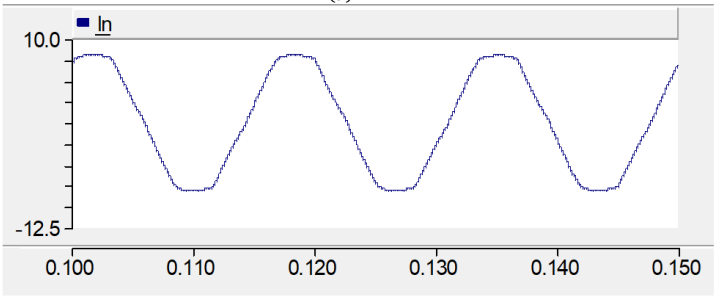

(b)

Figure 13. (a) Three-phase non-linear and unbalanced load current, (b) neutral current.

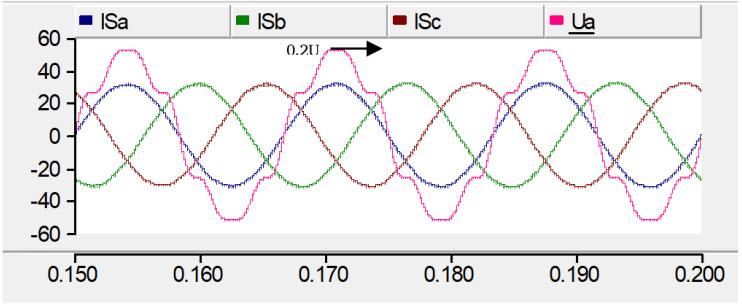

Figure 14. Compensated line currents and voltage of phase a.

3.3.1. *PV Compensating Operational Mode without Power Generation*

The performance of PV as just AF is described in this section to demonstrate the capability of the proposed system to compensate load current harmonics, eliminate the 4th wire current, and correct the power factor. In this part, no power is injected into the grid. As shown in Figure 14, the line currents drawn from the utility are sinusoidal and balanced. They are in phase with their related voltage. This shows the efficient usage of utility power. The line currents exhibit only high-frequency, low-amplitude harmonic components, ensuring that total harmonic distortion (THD) remains at approximately 0.88%. This indicates that the applied control strategy effectively minimizes harmonic distortions and improves power quality and grid compliance with IEEE standards.

3.3.2. *System Performance as both AF and Power Supply*

This section of the simulation assesses the system's response to variations in PV power due to changes in light intensity and temperature. Figure 14 illustrates three distinct stages caused by these variations:

- Stage 1 (0–0.2 sec): Light intensity is approximately 800 W/m^2, and temperature is around 35 ºC.
- Stage 2 (0.2–0.5 sec): Light intensity jumps to 1100 W/m^2 while temperature remains constant.
- Stage 3 (0.5–0.6 sec): Temperature drops sharply to 10 ºC, with light intensity unchanged.

As depicted in Figure 15, the PV array's P–V curves shift according to these stages, shown in Figure 16(a). The Boost converter's duty cycle adjusts dynamically to track the maximum power point (MPP) under each condition (Figure 16(b)). Additionally, Figure 16(c) presents the corresponding PV array voltage and current variations throughout the simulation.

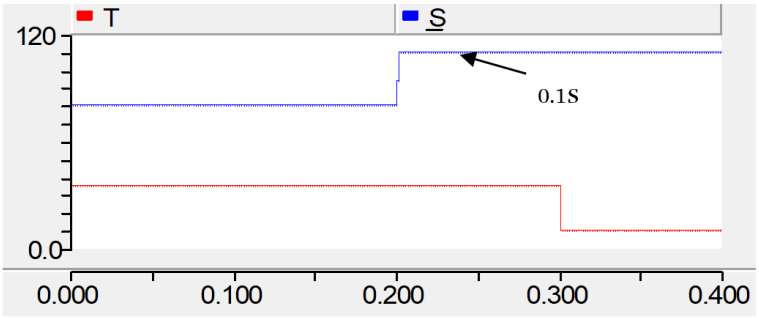

Figure 15. Diagram of variation in light intensity and temperature.

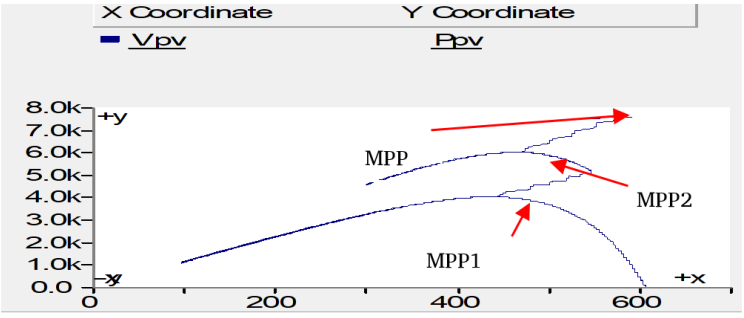

(a)

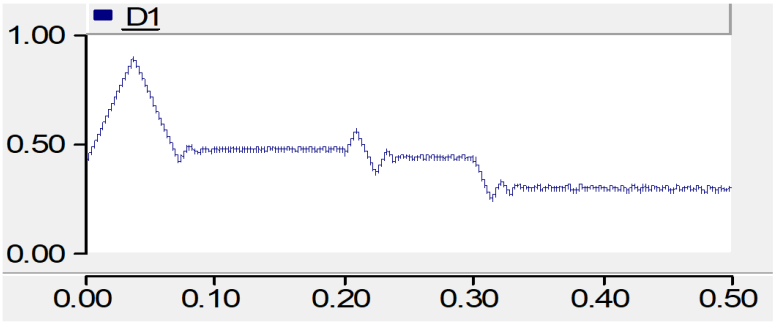

(b)

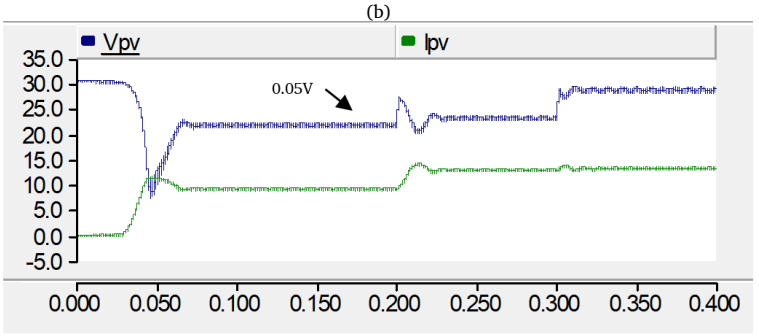

(c)

Figure 16. Variations of three stages (a) P-V curves of PV array, (b) duty cycle, (c) Voltage and current PV array.

The simulation outcomes for the three stages, presented in Figure 15, demonstrate that the PV system can operate simultaneously as an AF and a power source under unbalanced and non-sinusoidal voltage conditions. Figure 17 illustrates the active and reactive power injected by both the source and the PV array. The PV array provides the reactive power required by the load and also performs a peak-shaving function: as PV real power injection rises, the power supplied by the main source correspondingly decreases.

As shown in Figure 18, the PV system effectively compensates for load current harmonics across all stages, maintaining THD below 1%. Moreover, it eliminates neutral current, with the RMS value of the neutral line current recorded at 0.035 A (Figure 19). Detailed THD values of the source currents for all cases are summarized in Table 4.

The DC link voltage of the capacitor is shown in Figure 20 for the three stages. The capacitor voltage is precisely maintained at 1200V, corresponding to approximately three times the line voltage (380V). This regulation ensures stable energy storage and effective power conversion, optimizing system performance and operational efficiency.

Table 4. THD values.

	THD (i_{sa})%	THD (i_{sb})%	THD (i_{sc})%
Before compensation	21.24	15.63	14.52
After compensation ($P_{inj}=0$ kw)	0.57	0.65	0.88
After compensation ($P_{inj}=4$ kw)	0.76	0.66	0.7
After compensation ($P_{inj}=6$ kw)	0.82	0.75	0.77
After compensation ($P_{inj}=7.5$ kw)	1	0.9	0.93

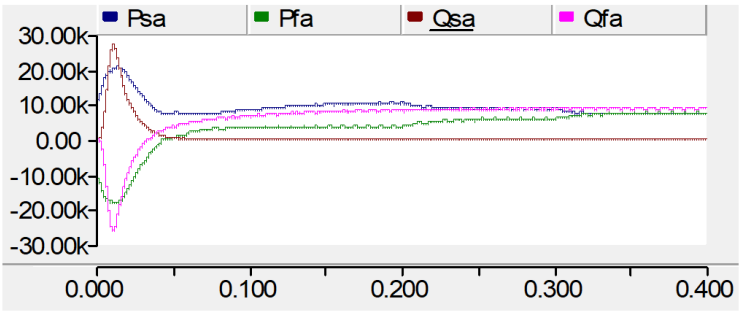

Figure 17. The source and PV active and reactive injected power.

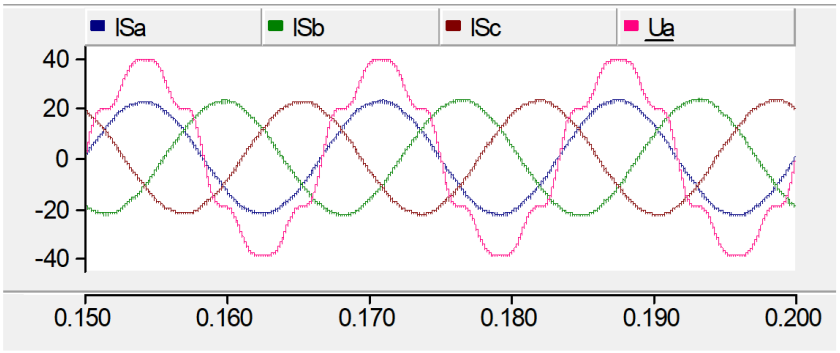

(a)

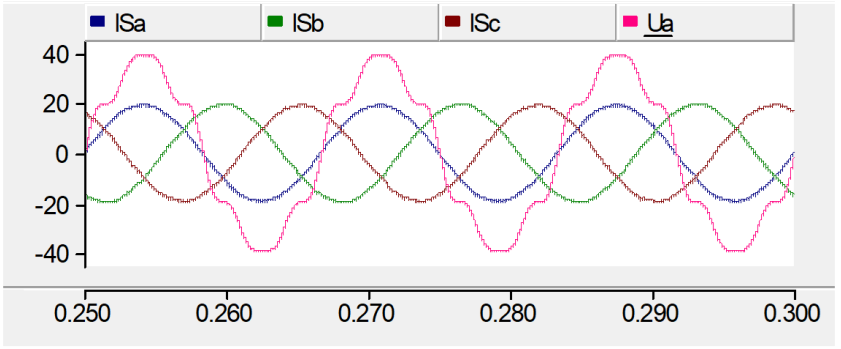

(b)

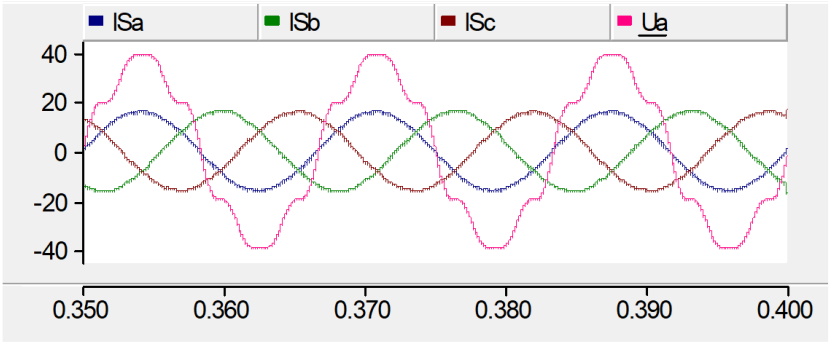

(c)

Figure 18. Compensated currents and utility voltage with balanced and non-sinusoidal voltage supply (a) stage one, (b) stage two, (c) stage three.

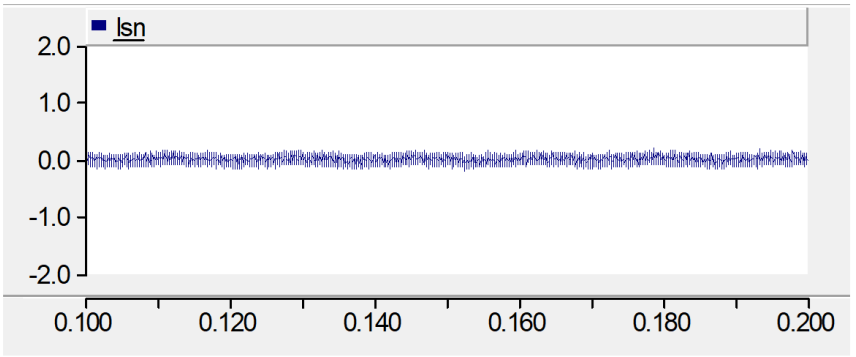

Figure 19. Neutral current after compensation.

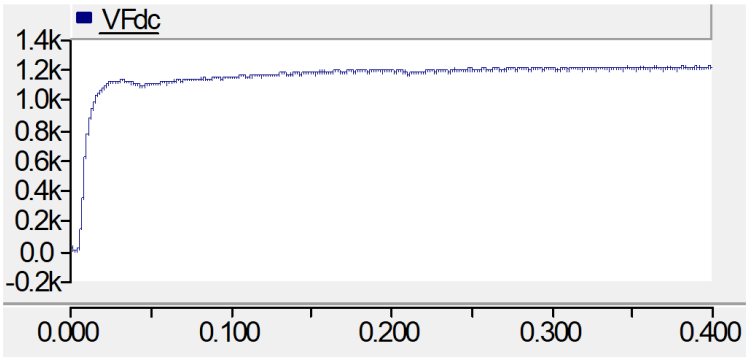

Figure 20. The DC link voltage.

3.4. Analysis of the results for the Proposed Enhanced Vectorial Theory Control System

The simulation results demonstrate the effectiveness of the enhanced vectorial control strategy in managing a grid-connected 4-wire PV-AF system under various operational conditions. The following key observations highlight the system's performance:

Harmonic Suppression and Power Factor Correction: The proposed PV-AF system effectively mitigates harmonic distortions, ensuring that THD remains below 1% across different PV power injection levels. The system maintains a unity power factor, indicating optimized active power utilization and minimal reactive power demand.

Neutral Current Compensation: Under unbalanced load conditions, the neutral current was significantly suppressed, reducing its RMS value to approximately 0.035. This confirms the APF functionality in addressing issues related to neutral current fluctuation in three-phase four-wire systems.

Adaptive PV Power Injection: The MPPT algorithm effectively tracks the MPP across varying solar irradiance and temperature levels, ensuring efficient energy conversion. The system dynamically adjusts real power injection, thus optimizing grid interaction and reducing the source's burden.

DC-Link Voltage Stability: The DC-link capacitor voltage was consistently regulated at 1200V, which is approximately three times the line voltage (380V), providing stable energy buffering for effective power compensation and injection.

Overall, the results validate the proposed enhanced vectorial control strategy, confirming its capability to enhance grid stability, harmonic suppression, neutral current elimination, and PV power utilization.

4. Comparative Results Analysis for the Two Proposed Control Strategies

Harmonic Suppression and Power Quality Improvement: The corrected p-q control strategy effectively maintains THD below 3%, ensuring harmonic suppression while compensating for current unbalance, reactive power demand, and neutral current fluctuations. The enhanced vectorial control theory, however, achieves a lower THD (approximately 0.88%), demonstrating superior harmonic mitigation under various operational conditions.

Neutral Current Compensation: The corrected p-q theory maintains the RMS neutral line current at 0.09, providing satisfactory neutral current suppression. The enhanced vectorial control-based system achieves a lower RMS neutral line current (0.035), indicating stronger compensation performance for neutral current elimination.

Adaptive PV Power Injection and MPPT Efficiency: The corrected p-q theory implementation operates under three PV power injection stages, efficiently tracking environmental variations. The system successfully injects real power alongside reactive power compensation to stabilize grid operations. The enhanced vectorial control theory-based system operates across four PV injection stages, offering enhanced adaptability in tracking the MPP across a wider range of irradiance and temperature variations.

DC-Link Voltage Stability: The corrected p-q theory system stabilizes DC-link voltage at 800V, ensuring sufficient energy buffering for compensation and PV power injection. The enhanced vectorial control system, however, maintains DC-link voltage at 1200V, approximately three times the line voltage (380V), indicating a more robust energy management strategy.

Source Current Regulation and Reactive Power Compensation: The corrected p-q theory system ensures balanced and sinusoidal source currents, providing compensation for unbalanced, nonlinear, and reactive load currents while achieving grid compliance. The enhanced vectorial control approach delivers enhanced performance, maintaining balanced and sinusoidal source currents while demonstrating optimized reactive power compensation, ensuring utility power factor correction, and efficient energy utilization. Table 5 shows a comparison between the two proposed control methods.

Results indicate that the proposed enhanced vectorial control offers superior power quality, making it more suitable for grid applications with strict harmonic constraints. Below is a comparative analysis in Table 6 comparing the corrected p-q control strategy and enhanced vectorial control from the present paper with other methods discussed in the referenced literature. This table considers key parameters such as harmonic suppression, power factor correction, neutral current elimination, MPPT efficiency, and DC-link stability. Based on Table 6, the Enhanced Vectorial Control strategy proposed in the present paper proves to be one of the most effective methods for harmonic suppression and grid stabilization, competing closely with Neural Network-Based and Meta-Heuristic approaches. However, its complexity and cost are higher compared to simpler Instantaneous p-q Theory or Fuzzy Logic-Based Controllers.

Table 5. Comparison between the two proposed control methods.

Control Strategy	Harmonic Suppression (THD)	Power Factor Correction	Neutral Current Reduction	DC-Link Stability
Corrected p-q Theory	Below 3%	Moderate	RMS = 0.09	stable
Enhanced Vectorial Control	Below 1%	Excellent	RMS = 0.035	stable

Table 6. Comparison between the proposed control methods with other methods in the referenced literature.

Control Method	Harmonic Suppression (THD)	Power Factor Correction	Neutral Current Reduction	MPPT Efficiency	DC-Link Stability	Complexity and Cost
Corrected p-q Theory (This Paper)	Below 3%	Moderate	RMS = 0.09	Efficient	800V	Medium
Enhanced Vectorial Control (This Paper)	Below 1%	Excellent	RMS = 0.035	Highly Efficient	1200V	High
Instantaneous p-q Theory [6]	Moderate (5-8%)	Good	Limited	Moderate	Variable	Low
Fuzzy Logic-Based APF [10]	Below 5%	Moderate	Moderate	Adaptive	Stable	Medium
Neural Network-Based Control [9]	Below 2%	Excellent	Strong	Self-Optimizing	Highly Stable	High
Hybrid AC/DC Microgrid Control [7]	Below 4%	Adaptive	Moderate	Good	Variable	Medium
Meta-Heuristic Algorithm-Based Filtering [20]	Below 1.5%	Excellent	Strong	High Adaptability	Highly Stable	High
Grid-Friendly Smart Inverter Control [21]	Below 3%	High	Moderate	Advanced MPPT	Stable	High

5. Conclusion

This paper proposes two control strategies: the corrected p-q control strategy and the enhanced vectorial control theory. The comparative analysis highlights the strengths and trade-offs between these two methods when applied to grid-connected FPV systems in three-phase four-wire distribution grids:

- The corrected p-q theory approach is effective in harmonic suppression, reactive power compensation, and adaptive PV power injection, ensuring stable power quality under dynamic environmental conditions.
- The enhanced vectorial control theory approach, however, offers superior harmonic suppression, improved neutral current elimination, and robust DC-link voltage stabilization, making it a more efficient solution for power management and grid stability enhancement.

Simulation results confirm that both methods significantly improve power quality, but vectorial control outperforms traditional techniques by reducing THD to 0.88% and enhancing neutral current mitigation. Future research should focus on real-world implementation, cost analysis, and experimental validation using hardware prototypes.

References

[1] J. Ebrahimi, and M. Abasi, "Design of a Power Management Strategy in Smart Distribution Networks with Wind Turbines and EV Charging Stations to Reduce Loss, Improve Voltage Profile, and Increase Hosting Capacity of the Network," *Journal of Green Energy Research and Innovation*, vol. 1, no. 1, pp. 1–15, 2024.

[2] N. Bagheri, M. A. Bahramian, and A. A. Ghadimi, "Optimal Capacitor Placement in Distributed Networks Polluted with Harmonics in the Presence of Wind Energy-Based Distributed Generation Sources," *Journal of Green Energy Research and Innovation*, vol. 1, no. 4, pp. 1–16, 2024.

[3] M. Shiravand, and A. Nahavandi, "Control and Improvement of Power Quality in Hybrid Three-Terminal AC/DC Microgrids," *Journal of Green Energy Research and Innovation*, vol. 1, no. 2, pp. 31–45, 2024.

[4] S. Khani, L. Mohammadian, and S. H. Hosseini, "Controlling a 4-Wire PV-AF System in Existence of Unbalanced and Distorted Supply Voltages," *20th Iranian Conference on Electrical Engineering (ICEE2012)*, pp. 473–478, 2012.

[5] M. E. Ali, S. Mahmud, M. O. Ali, and M. F. Ahmed, "PV-Based Active Harmonic Power Filter for Power Quality Analysis," *IOSR Journal of Electrical and Electronics Engineering*, vol. 18, no. 1, pp. 57–66, 2023.

[6] A. Khandelwal, and N. Joshi, "Implementation of Fuzzy Controller Based Active Filter for Harmonic Mitigation of Grid-Connected PV-System," *International Journal of Applied Power Engineering (IJAPE)*, vol. 13, no. 3, 539, 2024.

[7] M. Golla, K. Chandrasekaran, and S. P. Simon, "PV Integrated Universal Active Power Filter for Power Quality Enhancement and Effective Power Management," *Energy for Sustainable Development*, vol. 61, pp. 104–117, 2021.

[8] T. Green, and J. Marks, "Control Techniques for Active Power Filters," *IEE Proceedings - Electric Power Applications*, vol. 152, no. 2, pp. 369–381, 2005.

[9] F. Osorio, M. A. Mantilla, J. M. Rey, and J. F. Petit, "A Flexible Control Strategy for Multi-Functional PV Inverters with Load Compensation Capabilities Considering Current Limitations and Unbalanced Load Conditions," *Energies*, vol. 17, no. 17, 4218, 2024.

[10] J. Fu, T. Li, et al., "Three-Phase Four-Wire OPF-Based Collaborative Control of PV Inverter and ESS for Low-Voltage Distribution Networks with High Proportion PVs," *Frontiers in Energy Research*, vol. 8, 2021.

[11] R. Wagle, P. Sharma, C. Sharma, and M. Amin, "Optimal Power Flow Based Coordinated Reactive and Active Power Control to Mitigate Voltage Violations in Smart Inverter Enriched Distribution Network," *International Journal of Green Energy*, vol. 21, no. 2, pp. 359–375, 2023.

[12] M. Hajji, Z. Yahyaoui, M. Mansouri, H. Nounou, and M. Nounou, "Fault Detection and Diagnosis in Grid-Connected PV Systems Under Irradiance Variations," *Energy Reports*, vol. 9, pp. 4005–4017, 2023.

[13] S. Chen, and G. Heilscher, "Integration of Distributed PV into Smart Grids: A Comprehensive Analysis for Germany," *Energy Strategy Reviews*, vol. 55, 101525, 2024.

[14] S. Khani, S. H. Hosseini, and L. Mohammadian, "Application of the Vectorial Theory in PV-AF System for Load Supply and Harmonic Compensation with Unbalanced and Distorted Supply Voltages," *19th Iranian Conference on Electrical Engineering (ICEE2011)*, pp. 1–6, 2011.

[15] D. Murillo-Yarce, J. Alarcón-Alarcón, M. Rivera, C. Restrepo, J. Muñoz, C. Baier, and P. Wheeler, "A Review of Control Techniques in Photovoltaic Systems," *Sustainability*, vol. 12, no. 24, p. 10598, 2020.

[16] J. Hu, and K. Zhang, "Research on Flexible Control Technology of Photovoltaic and Energy Storage System," *2022 12th International Conference on Power and Energy Systems (ICPES)*, pp. 876–879, 2022.

[17] J. M. R. Dominguez, J. Riquelme, and S. Martinez, "New Trends in the Control of Grid-Connected Photovoltaic Systems for the Provision of Ancillary Services," *Energies*, vol. 15, p. 7934, 2022.
[18] K. Reham, A. Wael, and N. Mohamed, "Harmonic Analysis Comparison between PV Integration in High Voltage and Medium Voltage Networks," *American Journal of Engineering Research*, vol. 10, pp. 263–276, 2021.
[19] P. Rahmati Kahkha, A. HossienPour, and A. Khajeh, "Four-Switch Inverter Based Hybrid Power Filter Optimized by Meta-Heuristic Algorithm of SPEA," *International Journal of Industrial Electronics Control and Optimization*, vol. 6, no. 2, pp. 133–141, 2023.
[20] D. Murillo-Yarce, J. Alarcón-Alarcón, et al., "A Review of Control Techniques in Photovoltaic Systems," *Sustainability*, vol. 12, no. 24, 10598, 2020.
[21] Q. Peng, A. Sangwongwanich, Y. Yang, and F. Blaabjerg, "Grid-Friendly Power Control for Smart Photovoltaic Systems," *Solar Energy*, vol. 210, pp. 115–127, 2020.

Declaration of competing interest

The authors declare that they have no known competing financial interests or personal relationships that could have appeared to influence the work reported in this paper. The ethical issues, including plagiarism, informed consent, misconduct, data fabrication and/or falsification, double publication and/or submission, redundancy, have been completely observed by the authors.

Bibliography

Saeid Khani was born in Tabriz, Iran, 1984. He received his B.Sc. degree in electrical engineering from the University of Zanjan, Iran and M.Sc. and Ph.D. degrees in electrical engineering from the University of Tabriz, Iran in 2007, 2011 and 2023 respectively. His research interests include power electronic converters and power electronic application in renewable energy systems, power quality enhancement and facts.
Email: Saeid_khani82@yahoo.com
ORCID: 0009-0009-0956-2097
Contribution Statement: Formal analysis, Methodology, Software, Roles/Writing-original draft, Writing-review & editing.

Leila Mohammadian was born in Tabriz, Iran, in 1984. She received her B.S., M.S., and Ph.D. degrees in Electrical Engineering from the Department of Electrical and Computer Engineering, University of Tabriz, Tabriz, Iran, in 2007, 2011, and 2015, respectively. She has been with the Department of Electrical Engineering, Shab.C., Islamic Azad University, Shabestar, Iran, since 2011. She has been an Assistant Professor since 2015. She is the author of more than 60 journal and conference papers. Her current research interests include the analysis and control of power electronic converters and their applications, power quality enhancement and FACTS devices, application of control systems and theory in power engineering, and power system dynamics, renewable energy sources, and energy storage systems.
Email: le.mohammadian@iau.ac.ir
ORCID: 0000-0001-5202-1397
Contribution Statement: Conceptualization, Investigation, Methodology, Supervision, Writing-review & editing.